Tu *et al. J Mater Inf* 2022;2:13
**DOI:** 10.20517/jmi.2022.10

**Journal of Materials Informatics**

**Research Article**

**Open Access**

# CuB monolayer: a novel 2D anti-van't Hoff/Le Bel nanostructure with planar hyper-coordinate boron/copper and superconductivity

**Kaixiong Tu, Jinxing Gu, Linguo Lu, Shijun Yuan, Long Zhou, Zhongfang Chen***

Department of Chemistry, University of Puerto Rico, Rio Piedras Campus, San Juan, PR 00931, USA.

***Correspondence to:** Prof. Zhongfang Chen, Department of Chemistry, University of Puerto Rico, Rio Piedras Campus, 17 Ave. Universidad STE 1701, San Juan, PR 00931, USA. E-mail: zhongfang.chen1@upr.edu

**How to cite this article:** Tu K, Gu J, Lu L, Yuan S, Zhou L, Chen Z. CuB monolayer: a novel 2D anti-van't Hoff/Le Bel nanostructure with planar hyper-coordinate boron/copper and superconductivity. *J Mater Inf* 2022;2:13. https://dx.doi.org/10.20517/jmi.2022.10

**Received:** 24 Apr 2022 **First Decision:** 14 Jul 2022 **Revised:** 13 Aug 2022 **Accepted:** 23 Aug 2022 **Published:** 2 Sep 2022

**Academic Editor:** Xingjun Liu **Copy Editor:** Tiantian Shi **Production Editor:** Tiantian Shi

## Abstract

To achieve specific applications, it is always desirable to design new materials with peculiar topological properties. Herein, based on a $D_{2h}$ $B_2Cu_6H_6$ molecule with the unique chemical bonding of planar pentacoordinate boron (ppB) as a building block, we constructed an infinite CuB monolayer by linking $B_2Cu_6$ subunits in an orthorhombic lattice. The planarity of the CuB sheet is attributed to the multicenter bonds and electron donation-back donation, as revealed by chemical bonding analysis. As a global minimum confirmed by the particle swarm optimization method, the CuB monolayer is expected to be highly stable, as indicated by its rather high cohesive energy, absence of soft phonon modes, and good resistance to high temperature, and thus is highly feasible for experimental realization. Remarkably, this CuB monolayer is metallic and predicted to be superconducting with an estimated critical temperature ($T_c$) of 4.6 K, and the critical temperature could be further enhanced by tensile strains (to 21 K at atmospheric pressure).

**Keywords:** Planar pentacoordinate boron, planar heptacoordinate copper, copper boride monolayer, density functional calculations, superconducting

## INTRODUCTION

The discovery of molecules and materials with unique bonding characteristics is highly desirable to advance materials science from the perspective of both fundamental understanding and applications. With various exceptional properties, such as its electron deficiency, small covalent radius, and versatility in adopting $sp^2$ and $sp^3$ hybridization, as well as multi-center bonds, boron can form plenty of polymorphs with intriguing chemical bonding[1-8]. Various nanostructures of boron, such as boron fullerenes[6-9], two-dimensional (2D) sheets[2,4,5,10,11], nanotubes[3-12], and core-shell structures[13,14], have been extensively studied. Excitingly, by joint theoretical and experimental efforts, Piazza *et al.* discovered the highly stable quasi-planar $B_{36}$ cluster with a central hexagonal hole, providing the first evidence of the viability of single-atom layer boron sheets with hexagonal vacancies[15]. Notably, the recent fabrication of borophene monolayer[16-19] further elaborated the richness of boron chemistry and added a new member to the two-dimensional materials family[20-23]. With these structural diversities and concomitant fascinating properties, boron has been intensively employed to design new functional materials[16,24-26]. Moreover, a series of molecular wheels and 2D frameworks with unprecedented highly coordinated central transitional metal atoms have been either experimentally characterized or theoretically designed[27-30], which not only offers new methods to effectively modulate the structures and properties of boron polymorphs but also expands the frontier of boron chemistry. In organic chemistry, a well-known classical chemical model is the van't Hoff/Le Bel rule, following which a tetracoordinate carbon is of tetrahedral configuration[31,32], and thus a molecule containing tetracoordinate carbon in non-tetrahedral coordination is called anti-van't Hoff/Le Bel. However, nowadays, molecules or materials with planar hypercoordinate (higher than three) motifs[33,34] are generally considered as anti-van't Hoff/Le Bel structures. Note that most of the planar molecules or 2D nanomaterials mentioned above consist of anti-van't Hoff/Le Bel motifs, a special feature we address in this work.

Copper, an earth-abundant element, also forms various nanostructures. Among others, copper clusters have been extensively studied as building blocks of various organic and inorganic systems[35-38], and their catalytic activities have received great attention[39]; one-dimensional copper nanostructures (especially nanowires and nanorods) have shown great promise in various applications, such as in next-generation flexible and wearable electronics, functional electrodes, solar cells, and field emission devices[40]. Very recently, the yet-hypothetical free-standing 2D copper monolayer was predicted by Yang *et al.,* which adopts the hexagonal close-packed structure in the energetically most favorable configuration[41].

Copper can also form alloy structures with unique chemical bonding and novel properties. For example, Yang and coworkers predicted the $Cu_2Si$ monolayer featuring planar hexacoordinated silicon and copper[42], which was shortly synthesized and exhibited 2D Dirac nodal line fermions[43], and its superconductivity was predicted[44]. Moreover, recent theoretical studies predicted that quasi-planar $Cu_2Te$ layers are 2D topological insulators[45], and the planar $Cu_2Ge$ monolayer is a diamagnetic metal[46].

At the molecular scale, Li *et al.* thoroughly investigated planar tetracoordinate[47] and pentacoordinate[48] B embedded in hydrocopper complexes. Especially, $D_{5h}$ $Cu_5H_5B^-$ cluster showed high stability due to the optimal size match between pentagon $Cu_5H_5$ and B atom. These findings suggest that copper and boron platforms together might trigger novel topology and properties. In this respect, Jia *et al.* theoretically predicted that the CuB monolayer with planar hypercoordinate boron/copper is the lowest-energy configuration in the 2D space, and this metallic monolayer is a promising electrocatalyst for CO reduction to ethanol[49]. Zhou *et al.* investigated 2D copper borides by *ab initio* evolutionary searches[50], discovered three new metastable monolayer structures ($Cu_7B_{15}$, $CuB_3$, and $CuB_6$), and found the CuB monolayer as predicted by Jia *et al.* in the potential energy surface[49]. Excitingly, Zhou's group experimentally synthesized the $C_8B_{14}$ monolayer on the Cu(111) surface under an ultrahigh vacuum and revealed that the charge

transfer between Cu and B atoms plays an important role in stabilizing the 2D monolayer[51].

Inspired by the above exciting findings, we carried out a deep study of 2D CuB alloys using first-principles calculations combined with a global minimum search. Our systematic computations showed that the lowest-energy configuration of the copper boride (CuB) nanosheets possesses highly ordered anti-van't Hoff/Le Bel $B_2$@$Cu_6$ subunits (@ indicates that a $B_2$ unit is embedded in the $Cu_6$ ring) and has a fascinating chemical bonding with both planar heptacoordinate copper and planar pentacoordinate boron (ppB). The planar morphology of CuB monolayer mainly comes from its multicenter bonding characteristics and electron-donation-back-donation interactions. As a global minimum in 2D space, the CuB monolayer not only has remarkable mechanical properties but also is predicted to be a phonon-mediated superconductor with an estimated critical temperature ($T_c$) of 10 K. With large cohesive energy, kinetic stability, and high melting temperature, the newly predicted CuB monolayer has good potential for experimental realization.

## COMPUTATIONAL METHODS

For the $Cu_6B_2H_6$ molecule, full geometry optimization, electronic structure computations, and harmonic frequency analysis were carried out at the B3LYP/6-311+G(d,p)[52-54] level of theory utilizing the ORCA 4.0 program[55].

For the 2D CuB monolayer, density functional theory (DFT) computations were performed using the projector augmented wave (PAW) method[56,57] as implemented in the Vienna *ab initio* simulation package (VASP) code[58]. The Perdew-Burke-Ernzerhof exchange-correlation functional (PBE)[59] and a 600 eV energy cut-off were adopted. The geometric structures were fully optimized until the energy precision reached $10^{-6}$ eV and the atomic force was less than $10^{-3}$ eV/Å. During structure optimizations, the vacuum regions between layers were fixed to 15 Å to well separate the periodic images in the *z*-direction, whereas the *x* and *y* lattice vectors were fully relaxed. The Brillouin zone was sampled with a 10 × 8 × 1 Γ-centered Monkhorst-Pack *k*-point grid for geometry optimizations, while a larger grid (30 × 24 × 1) was used for self-consistent calculations. Since PBE tends to underestimate the band gaps, the screened hybrid Heyd–Scuseria–Ernzerhof functional (HSE06)[60], which typically gives more accurate band gap values, was used to increase the reliability of the electronic structure predictions.

To better understand the unique bonding and stabilizing mechanism in the CuB monolayer, we carefully examined the chemical bonding *via* deformation charge density (DCD) analysis, electron localization function (ELF)[61,62] analysis, and the solid state adaptive natural density partitioning (SSAdNDP)[63] method. On the fly, pseudopotentials, as implemented in the CASTEP code[64], were used to calculate the bond overlap population (BOP)[65] values.

To assess the mechanical properties of the CuB nanosheet, the elastic constants were calculated, and based on the obtained elastic modulus tensors, the in-plane Young's modulus and the Poisson's ratio were evaluated.

To evaluate the kinetic stability of 2D CuB structures, we performed phonon dispersion calculations based on the density functional perturbation theory (DFPT)[66] using the Phonopy code interfaced with VASP. During the phonon calculations, more stringent energy and force convergence criteria ($10^{-8}$ eV and $10^{-4}$ eV/Å, respectively) were used.

To assess the thermal stabilities of the 2D CuB monolayer, using the PAW method and PBE functional, we performed *ab initio* molecular dynamics (AIMD) simulations in the canonical NVT ensemble. In these AIMD simulations, the initial configurations of CuB monolayer with 3 × 2 supercell (24 Cu atoms and 24 B atoms) were annealed at different temperatures (300, 600, 900, 1200, and 1500 K, respectively), each MD simulation lasted for 15 *ps* (at a time step of 1.0 *fs*), and the temperature was controlled by using the Nosé–Hoover thermostat[67].

The particle swarm optimization (PSO) method, as implemented in the CALYPSO code, was employed for searching low-lying 2D CuB monolayers. In these calculations, the simulation cells containing total atoms of 2, 4, 6, and 8 were considered, and the population size and the number of generations were set to 30 and 50, respectively. The structural relaxations were performed at the PBE level of theory using the VASP code.

Using the Quantum Espresso (QE) package[68], we computed the phonon dispersion and the electron-phonon coupling (ECP) to investigate the phonon-mediated superconducting properties and estimate the superconducting critical temperature ($T_c$) of the 2D CuB monolayers (including those under external strains). In these calculations, the plane wave ultrasoft pseudopotentials and the LDA functional for exchange–correlation interaction were used to model the electron–ion interactions[69,70], and the VASP structures were re-optimized within QE. The kinetic energy cut-off and the charge density cut-off of the plane wave basis were chosen as 90 and 900 Ry, respectively. The self-consistent calculations were carried out using a 32 × 32 × 1 Monkhorst-Pack *k*-point mesh. The full Brillouin zone phonon spectra were calculated from the dynamical matrices and EPC matrix elements on a 4 × 4 × 1 q-point grid. The $T_c$ values were estimated based on the McMillan-Allen-Dynes formula.

## RESULTS AND DISCUSSION

### $Cu_6B_2H_6$ as the inspiring ppB species for 2D monolayer

Our design of the periodic 2D CuB monolayer was inspired by the $Cu_6B_2H_6$ molecule, which contains planar penta-coordinated boron (ppB) motifs. $Cu_6B_2H_6$ has a singlet ground state with $D_{2h}$ symmetry [Figure 1A]. At the B3LYP/6-31+G* level of theory, $Cu_6B_2H_6$ is a local minimum with the lowest vibrational frequency of 66.1 $cm^{-1}$. In this molecule, the center B atom binds with four peripheral Cu atoms and its adjacent B atom, leading to the formation of ppB species. The distances between the ppB atom and Cu atoms (2.03 and 2.05 Å) are slightly smaller than the standard Cu-B single bond (2.06-2.20 Å)[71,72], while the Cu-Cu bond lengths (2.43 and 2.58 Å) are close to that in metallic Cu (2.56 Å). Especially, the B–B bond length (1.54 Å) is shorter than that of diborane (1.76 Å), close to diborene[73] (1.56 Å), and longer than diboryne[74,75] (1.46 Å), which suggests the partial double bond feature of the B-B bond.

To gain further insights into the bonding features of $Cu_6B_2H_6$, we calculated the atomic charges and the Wiberg bond index (WBI)[76-78] by natural bonding orbital (NBO) computations[79,80] at the B3LYP/6-311+G(d,p) level of theory. Since $D_{5h}$ $BH_5$ is isoelectronic to $D_{4h}$ $CH_4$[81], the pentacoordinate B can also be stabilized by σ donation group or delocalization of B $p_z$ electrons, as in the case of tetracoordinate carbon. Based on the charges obtained by natural population analysis (NPA)[82], the natural electron configuration of ppB is $2s^{0.83}2p_x^{1.07}2p_y^{0.89}2p_z^{0.88}$, and the center B atoms gains 0.70 |e| from neighboring Cu atoms, which donates 0.21 and 0.60 |e|, respectively, while H atoms play as charge compensate group. The WBIs for ppB-Cu bonds are 0.38 and 0.40, respectively, whereas the WBI for ppB-ppB bond is 1.92, which indicates that the partial bonds are formed between ppB and its adjacent Cu atoms, while the B-B interactions have double-bond characteristics. These give the ppB center a total WBI of 3.92.

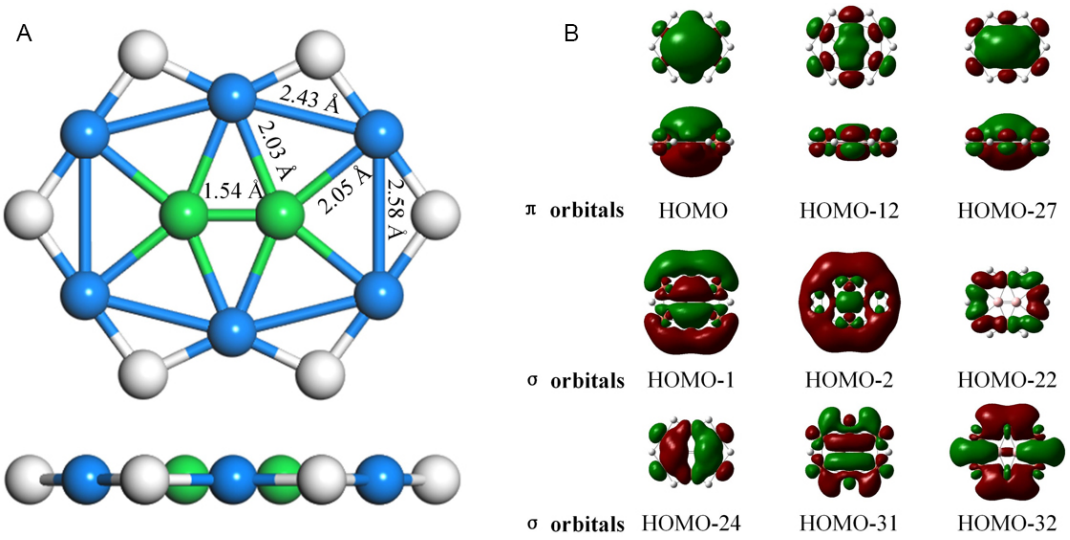


**Figure 1.** (A) Top and side views of the optimized structure of $Cu_6B_2H_6$ molecule. The blue, green, and white balls represent Cu, B, and H atoms, respectively. The bond lengths (in Å) of the representative chemical bonds are given in black. (B) The canonical molecular orbitals of $Cu_6B_2H_6$ molecule.

Additionally, we examined the canonical molecular orbitals of the $Cu_6B_2H_6$ molecule to better understand its stabilization mechanism. As shown in Figure 1B, the central B atom and the surrounding Cu atoms are involved in the highly delocalized π (HOMO, HOMO-13, and HOMO-27) and σ (HOMO-1, HOMO-2, HOMO-22, HOMO-24, HOMO-31, and HOMO-32) orbitals; thus, it is these well-delocalized electrons that help retain the B center and peripheral Cu atoms in the same plane. Especially, the electron donation from the central B atoms to the surrounding Cu atoms (HOMO-1) and back-donation from the peripheral Cu atoms to the embedded B atoms (HOMO) play an important role in stabilizing ppB in the $Cu_6B_2H_6$ molecule.

### Geometric structure of the CuB monolayer

The exceptional chemical bonding of the ppB containing $Cu_6B_2H_6$ inspired us to design a new 2D planar structure, namely CuB monolayer. The CuB monolayer has a highly symmetric structure with an orthorhombic lattice with space group *Cmmm* (No. 65) [Figure 2A]. The unit cell of the CuB monolayer consists of four B and four Cu atoms, and the optimized lattice parameters are $a$ = 4.84 Å and $b$ = 6.16 Å, respectively. Similar to the $Cu_6B_2H_6$ molecule, each B atom in the CuB monolayer binds with the four nearest Cu atoms and one adjacent B atom, forming a $B_2$@$Cu_6$ subunit in the same plane. In the meantime, one Cu atom is shared by three $B_2$@$Cu_6$ subunits with a heptacoordination environment, including three Cu atoms and four B atoms. In the CuB monolayer, the Cu-B bond lengths (2.05 and 2.01 Å) are quite close to those of the $Cu_6B_2H_6$ molecule, whereas the B-B bond length (1.64 Å) deviates a little from that of $Cu_6B_2H_6$ molecule, but it is comparable to that in borophene (1.65–1.87 Å)[25,26].

To elucidate the unique bonding nature and stabilizing mechanism in the CuB monolayer, we plotted the deformation charge density (DCD), which was obtained by subtracting the charge density of isolated Cu and B atoms within the CuB monolayer [Figure 2B]. There is significant electron transfer from the 4s orbital of Cu atoms to B atoms, and the transferred electrons are delocalized inside the $B_2$@$Cu_6$ subunits, contributing to the stabilization of the copper boride systems. According to Hirschfeld population analysis[83], each Cu atom transfers 0.20 e to the nearby B atoms, suggesting the considerable ionization of Cu atoms. We further performed the bond overlap population (BOP) analysis to investigate the nature of

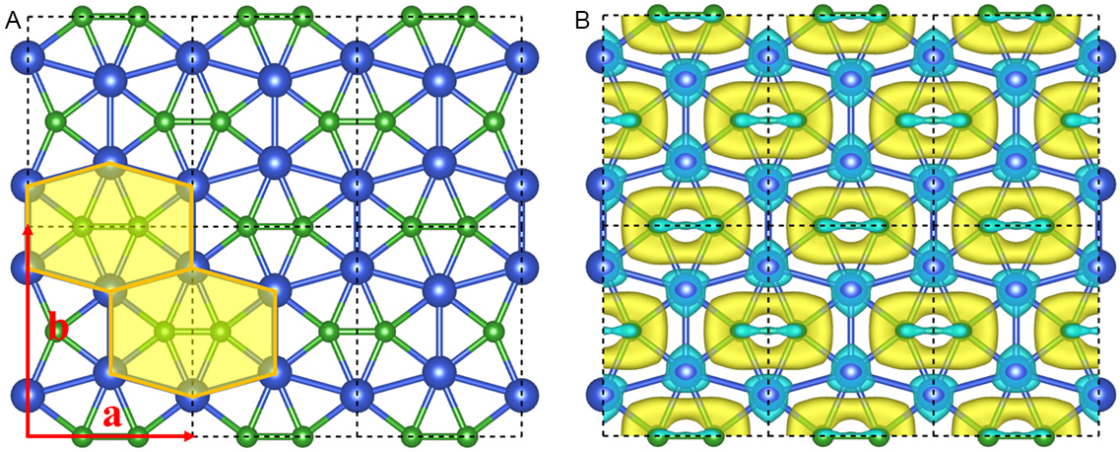


**Figure 2.** (A) Top and side views of the optimized structure of the CuB monolayer. The black dashed lines denote a unit cell; *a* and *b* represent the lattice vectors; and orange-filled hexagons are guidelines for the $B_2$@$Cu_6$ subunit. (B) The deformation charge density of CuB monolayer. Cyan and yellow represent electron-deficient and -rich regions, respectively. The isosurface value is 0.01 e/au.

chemical bonding. Note that a high BOP value denotes a larger covalency, while a low BOP value indicates a stronger ionicity. The B-B bonds have large BOP values (1.39), indicating a strong covalent bonding interaction. The BOP value of Cu-B bonds (0.43) is moderate, indicating a partial ionic and partial covalent bond interaction.

The electron localization function (ELF) provides a (local) measure of electron localization in molecules and solids and is a widely used tool for chemical bond classification and for understanding atomic structures. The ELF ranges from 0 to 1, where regions close to 0 represent very low charge density, the regions close to 1 correspond to perfect localization or denote strongly covalent bonding electrons, and the regions with 0.5 characterize a homogeneous electron gas. In the CuB monolayer, the electrons are well localized on B-B and Cu-B bonds [Figure 3], indicating the dominant covalent interactions inside each $B_2$@$Cu_6$ subunit, which is consistent with DCD analysis. While the electrons are well delocalized around Cu atoms, the whole Cu frameworks are in the color corresponding to the values around 0.44, implying the robust connection between Cu atoms, which is vital to electronically stabilize these 2D Cu-B networks. This electron transfer mechanism helps to stabilize the 2D copper boride systems. Moreover, the synergetic electron donation and back-donation interactions between the Cu and B atoms, as revealed in the $Cu_6B_2H_6$ molecule, contribute to the stabilization of the ppB configuration in the CuB monolayer.

Note that our newly constructed CuB monolayer inspired by the ppB containing $Cu_6B_2H_6$ molecule is the same Cu-B monolayer as recently predicted by Jia *et al.*, and our ELF analysis also agrees well with their finding[49].

We further analyzed the chemical bonding pattern of the CuB monolayer using the SSAdNDP method, which can interpret chemical bonding in terms of classical lone pairs and two-center bonds, as well as multicenter delocalized bonds[63]. Figure 4 presents the vital multicenter chemical bonding. Each unit cell of the CuB monolayer contains 12 lone pairs of *d*-type electrons on four Cu atoms, eight three-center-two-electron (3c-2e) Cu-B-Cu σ bonds, six 8c-2e $B_2$@$Cu_6$ σ bonds, and two 8c-2e $B_2$@$Cu_6$ π bonds, accounting for 56 valence electrons per unit cell. The reckoned bonding figure is consistent with the symmetry of the CuB monolayer. Hence, the abundance of multicenter delocalized σ and π bonds endows the CuB monolayer with high stability and planarity.

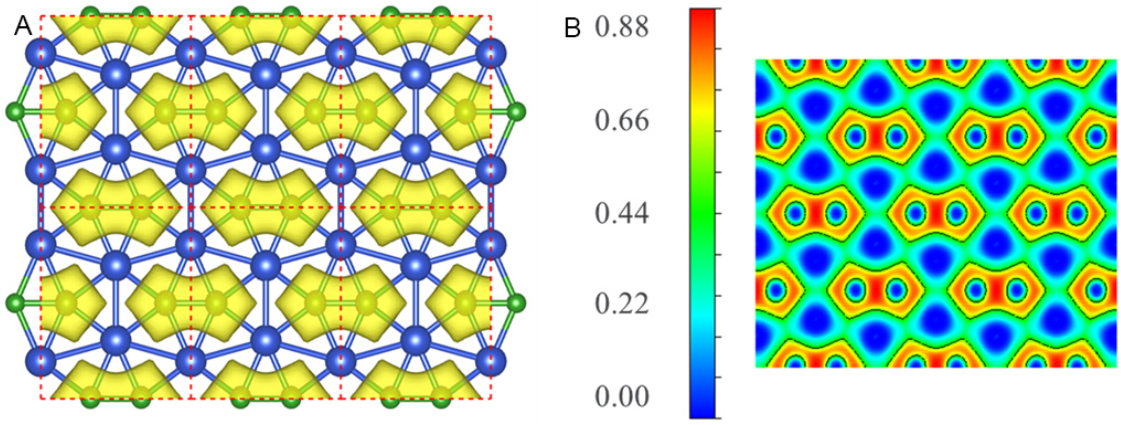


**Figure 3.** (A) Isosurface of electron localization function plotted with the value of 0.5 au and (B) ELF maps sliced perpendicular to (001) direction of CuB monolayer. In the ELF maps, the red and blue colors refer to the highest value (0.88) and the lowest value (0.00) of ELF, indicating electron accumulation and depletion in different colored regions, respectively.

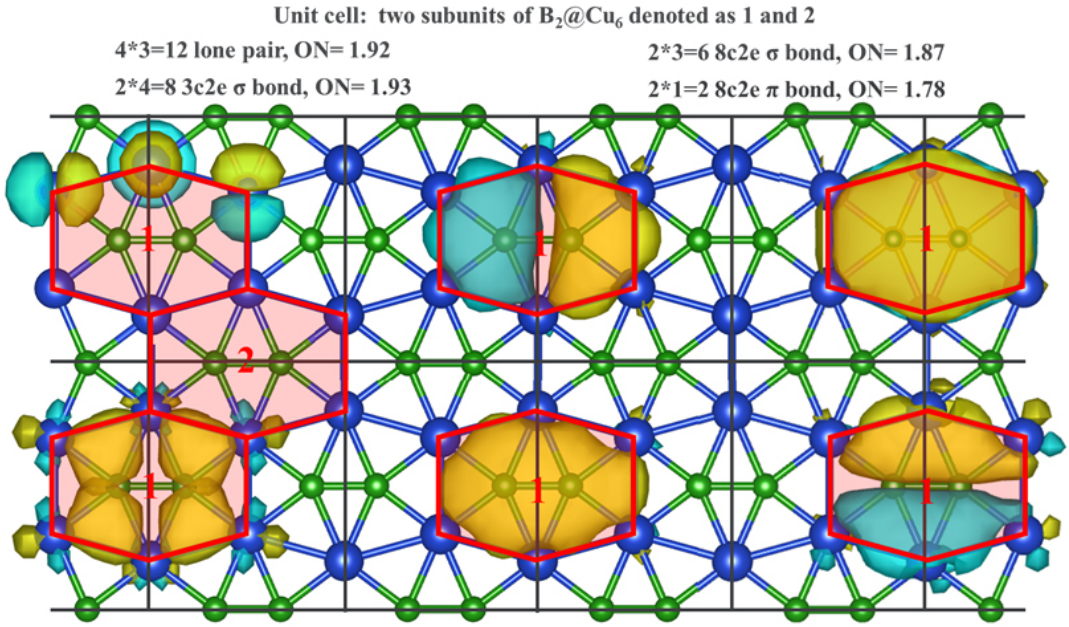


**Figure 4.** Schematic of the chemical bonding pattern by SSAdNDP method for the CuB monolayer.

### Stability of the CuB monolayer

We first evaluated the thermodynamic stability (by computing its cohesive energy) and kinetic stability (by examining its phonon dispersion along the high-symmetry lines in the first Brillouin zone). The obtained results are essentially the same as those reported by Jia *et al.*[49]; thus, they are not discussed here.

We then assessed the thermal stability of the CuB monolayer. Throughout 15 *ps* AIMD simulations up to 1200 K, the framework of the CuB sheet is well kept in its original configuration, and the $B_2$@$Cu_6$ subunits only have slight out-of-plane distortions [Figure 5A and B]. However, the $B_2$@$Cu_6$ subunits break at an extremely high temperature of 1500 K where B tends to form a chain structure [Figure 5C]. The well-maintained geometries at the high temperature up to 1200 K indicate the high thermal stability of the CuB monolayer. Additionally, we performed simulated annealing from the distorted structures obtained by

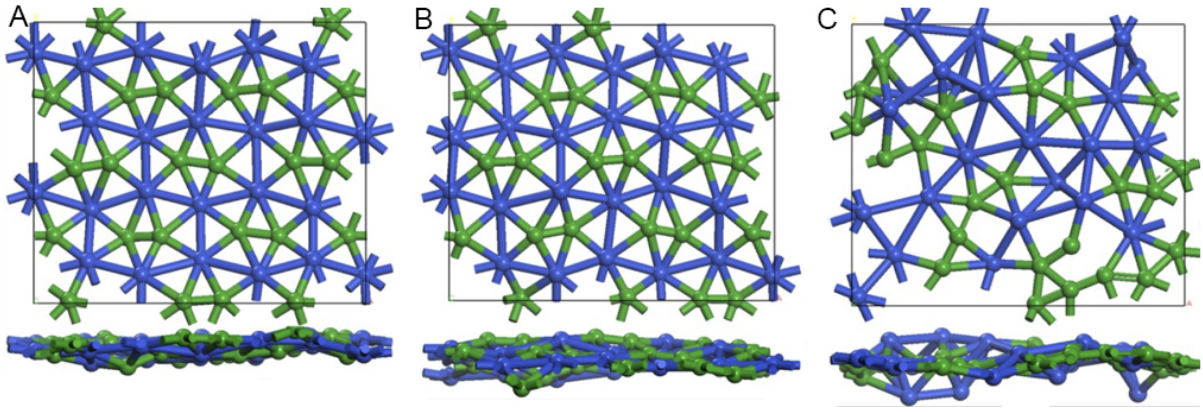


**Figure 5.** A snapshot of equilibrium structure of CuB monolayer at the end of 15 ps *ab initio* molecular dynamics simulations at different temperatures: (A) 900 K; (B) 1200 K; and (C) 1500 K.

AIMD at 900 and 1200 K, and these distorted structures can easily recover to their initial configurations, indicating the high phase stability of the CuB monolayer.

We further evaluated the mechanical properties of the CuB monolayer by computing its elastic constants. Its elastic constants, i.e. $C_{11} = C_{22} = 138.65$ N/m, $C_{12} = 45.35$ N/m, and $C_{66} = 55.49$ N/m, well satisfy the mechanical stability criteria for an orthorhombic 2D sheet ($C_{11}C_{22} > C_{12}^2$, $C_{66} > 0$). The in-plane Young's moduli along *a* and *b* directions can be computed by $Y_a = Y_b = (C_{11}C_{22} - C_{12}^2)/C_{22} = 123.81$ N/m, smaller than that of graphene (332 N/m)[84] and close to that of $MoS_2$ monolayer (128 N/m)[85], which suggests that the CuB monolayer has strong mechanical stability and is promising for mechanical applications. Additionally, the Poisson's ratio of the CuB monolayer can be calculated as $\nu_a = \nu_b = C_{12}/C_{11} = 0.33$ in both *a* and *b* directions; these values are larger than the corresponding ones for graphene (0.17)[86] and h-BN (0.23)[87] and are comparable with the Poisson's ratio for $MoS_2$ (0.29)[88].

Moreover, a comprehensive global minimum search was carried out for CuB by employing the PSO method. The computations give two low-lying configurations of 2D CuB, which are labeled CuB-I and CuB-II, respectively [Figure 6A and B]. Actually, CuB-I is the ppB-containing CuB monolayer, as discussed above. The structure of CuB-II (*Pmmn*, No. 59) can be described as an alternating zigzag chain of Cu atoms and a linear chain of B atoms, which is dynamically stable without any appreciable imaginary frequency [Figure 6C]. Our DFT computations showed that CuB-I is 94 meV per atom lower in energy than CuB-II; thus, our designed CuB monolayer (CuB-I) is indeed the global minimum structure in the 2D space.

### Electronic properties of the CuB monolayer

We also investigated the band structure of the CuB monolayer by HSE functional, and essentially the same results as those by Jia *et al.*[49] were obtained; thus, detailed discussions are not given here. Briefly, there are three band lines across the Fermi level, and therefore CuB monolayer is metallic.

The projected density-of-states (PDOS) show that both B-*p* states and Cu-*d* states are dominant at the peaks of DOS around the Fermi level, indicating the highly hybrid B and Cu orbitals nearby the Fermi level, which further supports the strong band interactions between Cu and B atoms in the CuB framework [Figure 7]. The high density of electron states around the Fermi level suggests that sufficient electrons are available to participate in the electronic transport, thus contributing to the outstanding electric conductivity of the CuB monolayer. The concomitant electric conductivity is consistent with the well-delocalized electrons, as

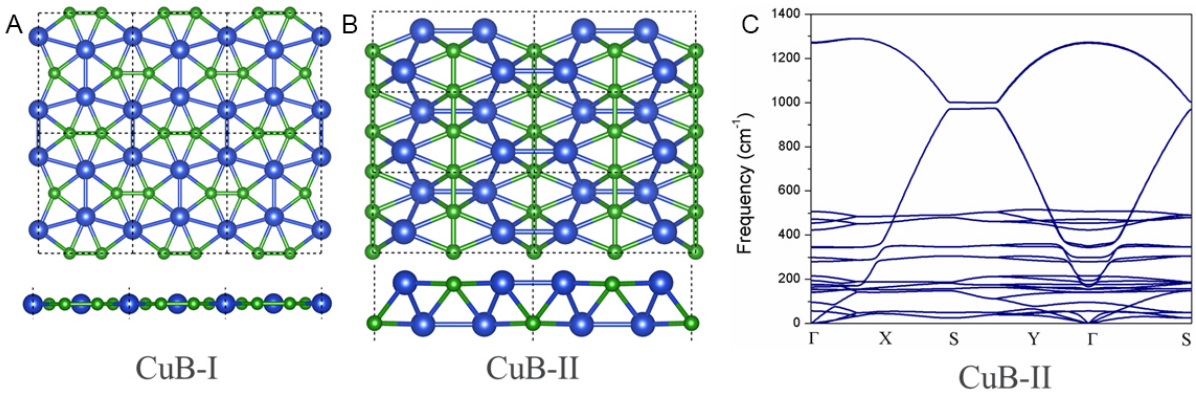


**Figure 6.** Two low-energy isomers of 2D CuB (A, B) and phonon spectrum of fully optimized CuB-II monolayer (C) computed at PBE functional.

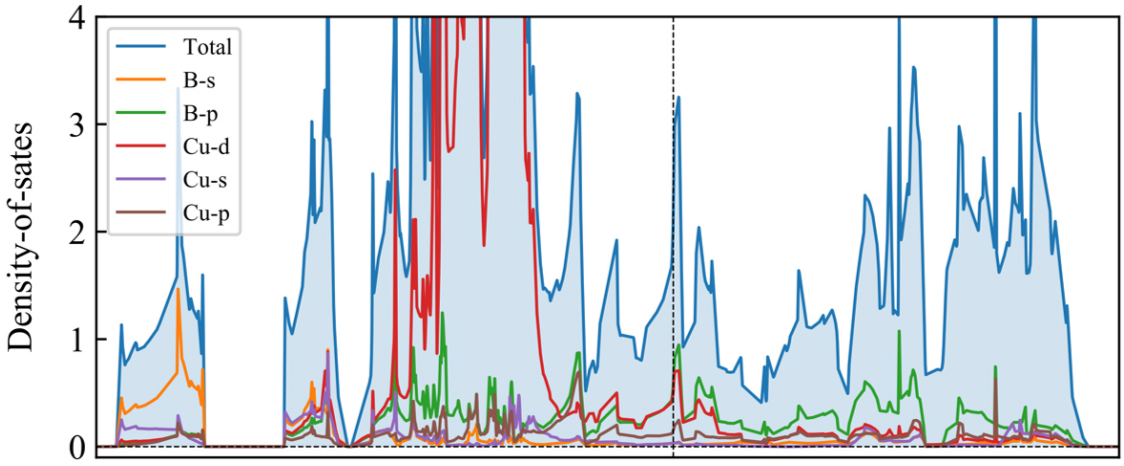


**Figure 7.** Total and partial density of states of the CuB monolayer.

revealed by our ELF and DCD analyses in this study.

### Superconductivity of the CuB monolayer

Inspired by the recently discovered superconductor $MgB_2$ with a high $T_c$ of 39 K[89], we theoretically calculated the electron–phonon coupling (EPC) and investigated the potential superconductivity of 2D CuB nanosheets. The component Cu is a heavy element, while B is a light element. Although CuB and $MgB_2$ have completely different geometric structures, they do share some similar properties: the metallic nature with substantial electronic states at the Fermi level and the existence of strong covalent bonding[90]. Thus, we expected that the CuB monolayer might be superconducting.

Using the Quantum Expresso (QE) code, we first calculated the phonon dispersion of the CuB monolayer. The QE-calculated phonon dispersion from QE is consistent with the VASP result discussed above, which confirms the reliability of our approach.

Based on the phonon dispersions obtained by QE, we calculated the electron–phonon coupling (ECP) and further investigated the potential superconductivity of the CuB monolayer. The superconducting temperature ($T_c$) was estimated by the Allan–Dynes-modified McMillan's approximation[91] of the

Eliashberg equation:

$$T_c = \frac{\varpi_{log}}{1.2} \exp\left[-\frac{1.04(1+\lambda)}{\lambda - \mu*(1+0.62\lambda)}\right]$$

where μ* is the Coulomb pseudopotential, λ is the overall electron–phonon coupling strength computed from the frequency-dependent Eliashberg spectral function $\alpha^2F(\omega)$, and $\omega_{log}$ is the logarithmic average phonon frequency. Note that this method has been widely used to predict superconductive 2D monolayers[44,92-94].

Since no exact method is available to determine the parameter μ* yet, here we estimated the μ* value by comparing the calculated $T_c$ with the experimentally known $MgB_2$ results. If μ* is set as 0.05, the $T_c$ of 36.9 K for $MgB_2$ with a λ of 0.71 is obtained, which is in good agreement with the experimental $T_c$ value (40 K) and λ value (~ 0.75)[95]. Thus, μ* = 0.05 was used to estimate $T_c$ for the 2D CuB monolayer.

Using the above-determined μ* value (0.05), the EPC parameter λ was calculated to be 0.51, suggesting a strong EPC effect; notably, the estimated superconducting critical temperature $T_c$ is as high as 4.6 K, which is higher than those of the previously reported $Y_2C$ (0.9 K)[96] and $Co_2C$ (3.4 K)[97] monolayers and is comparable to that of the $AlB_6$ (4.7 K) nanosheet[98].

Previous literature demonstrates that tensile strain may greatly influence the superconducting property[99]. Thus, we examined the strain effect for the CuB monolayer. Our computations showed that the CuB nanosheet is stable under strains of 0% ≤ ε ≤ 10%. Remarkably, the predicted superconducting $T_c$ reaches its highest temperature of 21 K when a tensile strain of 10% is adopted. These results suggest that the CuB nanosheets could be potentially utilized in future superconducting applications.

## CONCLUSION

Inspired by the bonding pattern of the $B_2Cu_6H_6$ molecule, we predicted the ppB-containing 2D CuB sheet by DFT computations, *ab inito* molecular dynamics simulations, and a comprehensive crystal structure search. The global minimum CuB monolayer is thermodynamically, dynamically, mechanically, and thermally stable. The electron donation and back donation between Cu and B atoms contribute to stabilizing ppB in the CuB monolayer. Young's modulus analysis showed that the CuB monolayer has promising mechanical properties. This CuB monolayer material is metallic and predicted to be phonon-mediated superconducting with an estimated critical temperature (*T*c) of 4.6 K. With the advancement of experimental techniques in fabricating 2D materials, we strongly believe that the CuB monolayer could be synthesized experimentally on some suitable substrate. Together with the progress recently achieved[49-51], this work could open a new branch of 2D copper boride layers with exceptional structures and fascinating properties.

## DECLARATIONS

### Authors' contributions

Conceptualization, investigation, writing - original draft: Tu K
Conceptualization, supervision, resources, writing - review & editing: Chen Z
Investigation, data analysis and interpretation: Gu J, Lu L, Yuan S, Zhou L

### Availability of data and materials

Not applicable.

**Financial support and sponsorship**

This work was supported by the NSF Centre for the Advancement of Wearable Technologies (Grant 1849243) and by NASA (Grant Number 80NSSC19M0236). A portion of the calculations used the resources of the Compute and Data Environment for Science (CADES) at ORNL and of the National Energy Research Scientific Computing Centre, which are supported by the Office of Science of the U.S. DOE under Contract No. DE-AC05-00OR22750 and DE-AC02-05CH11231, respectively. Some of the work was performed at the Center for Nanophase Materials Sciences, a U.S. DOE Office of Science User Facility.

**Conflicts of interest**

All authors declared that there are no conflicts of interest.

**Ethical approval and consent to participate**

Not applicable.

**Consent for publication**

Not applicable.



## REFERENCES

1. Balakrishnarajan MM, Hoffmann R. Electron-deficient bonding in rhomboid rings. *J Am Chem Soc* 2004;126:13119-31. DOI PubMed
2. Tang H, Ismail-Beigi S. Novel precursors for boron nanotubes: the competition of two-center and three-center bonding in boron sheets. *Phys Rev Lett* 2007;99:115501. DOI PubMed
3. Yang X, Ding Y, Ni J. Ab initio prediction of stable boron sheets and boron nanotubes: structure, stability, and electronic properties. *Phys Rev B* 2008:77. DOI
4. Penev ES, Bhowmick S, Sadrzadeh A, Yakobson BI. Polymorphism of two-dimensional boron. *Nano Lett* 2012;12:2441-5. DOI PubMed
5. Wu X, Dai J, Zhao Y, Zhuo Z, Yang J, Zeng XC. Two-dimensional boron monolayer sheets. *ACS Nano* 2012;6:7443-53. DOI PubMed
6. Zhai HJ, Zhao YF, Li WL, et al. Observation of an all-boron fullerene. *Nat Chem* 2014;6:727-31. DOI PubMed
7. Sergeeva AP, Popov IA, Piazza ZA, et al. Understanding boron through size-selected clusters: structure, chemical bonding, and fluxionality. *Acc Chem Res* 2014;47:1349-58. DOI PubMed
8. Zhang Z, Penev ES, Yakobson BI. Two-dimensional boron: structures, properties and applications. *Chem Soc Rev* 2017;46:6746-63. DOI
9. Szwacki N, Sadrzadeh A, Yakobson BI. B80 fullerene: an Ab initio prediction of geometry, stability, and electronic structure. *Phys Rev Lett* 2007;98:166804. DOI PubMed
10. Liu Y, Penev ES, Yakobson BI. Probing the synthesis of two-dimensional boron by first-principles computations. *Angew Chem Int Ed Engl* 2013;52:3156-9. DOI PubMed
11. Zhang H, Xie Y, Zhang Z, et al. Dirac nodal lines and tilted semi-dirac cones coexisting in a striped boron sheet. *J Phys Chem Lett* 2017;8:1707-13. DOI PubMed
12. Singh AK, Sadrzadeh A, Yakobson BI. Probing properties of boron alpha-tubes by Ab Initio calculations. *Nano Lett* 2008;8:1314-7. DOI PubMed
13. Zhao J, Wang L, Li F, Chen Z. B(80) and other medium-sized boron clusters: core-shell structures, not hollow cages. *J Phys Chem A* 2010;114:9969-72. DOI
14. Li F, Jin P, Jiang DE, et al. B80 and B101-103 clusters: remarkable stability of the core-shell structures established by validated density functionals. *J Chem Phys* 2012;136:074302. DOI PubMed
15. Piazza ZA, Hu HS, Li WL, Zhao YF, Li J, Wang LS. Planar hexagonal B(36) as a potential basis for extended single-atom layer boron sheets. *Nat Commun* 2014;5:3113. DOI PubMed
16. Mannix AJ, Zhou XF, Kiraly B, et al. Synthesis of borophenes: anisotropic, two-dimensional boron polymorphs. *Science* 2015;350:1513-6. DOI PubMed PMC
17. Feng B, Zhang J, Zhong Q, et al. Experimental realization of two-dimensional boron sheets. *Nat Chem* 2016;8:563-8. DOI PubMed
18. Kiraly B, Liu X, Wang L, et al. Borophene synthesis on Au(111). *ACS Nano* 2019;13:3816-22. DOI PubMed

19. Wu R, Drozdov IK, Eltinge S, et al. Large-area single-crystal sheets of borophene on Cu(111) surfaces. *Nat Nanotechnol* 2019;14:44-9. DOI PubMed
20. Xie SY, Wang Y, Li XB. Flat Boron: a new cousin of graphene. *Adv Mater* 2019;31:e1900392. DOI PubMed
21. Xie Z, Meng X, Li X, et al. Two-dimensional borophene: properties, fabrication, and promising applications. *Research (Wash D C)* 2020;2020:2624617. DOI PubMed PMC
22. Kaneti YV, Benu DP, Xu X, Yuliarto B, Yamauchi Y, Golberg D. Borophene: two-dimensional boron monolayer: synthesis, properties, and potential applications. *Chem Rev* 2022;122:1000-51. DOI PubMed
23. Ou M, Wang X, Yu L, et al. The emergence and evolution of borophene. *Adv Sci (Weinh)* 2021;8:2001801. DOI PubMed PMC
24. Zhang Z, Yang Y, Gao G, Yakobson BI. Two-dimensional boron monolayers mediated by metal substrates. *Angew Chem* 2015;127:13214-8. DOI PubMed
25. Xu SG, Li XT, Zhao YJ, et al. Two-dimensional semiconducting boron monolayers. *J Am Chem Soc* 2017;139:17233-6. DOI PubMed
26. Li W, Chen X, Jian T, Chen T, Li J, Wang L. From planar boron clusters to borophenes and metalloborophenes. *Nat Rev Chem* 2017:1. DOI
27. Romanescu C, Galeev TR, Li W, Boldyrev AI, Wang L. Aromatic metal-centered monocyclic boron rings: Co©B8− and Ru©B9−. *Angew Chem* 2011;123:9506-9. DOI PubMed
28. Popov IA, Jian T, Lopez GV, Boldyrev AI, Wang LS. Cobalt-centred boron molecular drums with the highest coordination number in the CoB16- cluster. *Nat Commun* 2015;6:8654. DOI PubMed PMC
29. Zhang H, Li Y, Hou J, Tu K, Chen Z. FeB6 monolayers: the Graphene-like material with hypercoordinate transition metal. *J Am Chem Soc* 2016;138:5644-51. DOI PubMed
30. Zhang H, Li Y, Hou J, Du A, Chen Z. Dirac state in the $FeB_2$ monolayer with graphene-like boron sheet. *Nano Lett* 2016;16:6124-9. DOI PubMed
31. Hoff V, Henricus J. Sur les formules de structure dans l'espace. *Archives néerlandaises des sciences exactes et naturelles* 1874; 9:445-454. DOI
32. Bel L, Achille J. Sur les relations qui existent entre les formules atomiques des corps organiques et le pouvoir rotatoire de leurs dissolutions. *Bulletin de la Société Chimique de Paris* 1874; 22:337-347. DOI
33. Yang LM, Ganz E, Chen Z, Wang ZX, Schleyer Pv. Four decades of the chemistry of planar hypercoordinate compounds. *Angew Chem Int Ed Engl* 2015;54:9468-501. DOI PubMed
34. Wang Y, Li Y, Chen Z. Planar hypercoordinate motifs in two-dimensional materials. *Acc Chem Res* 2020;53:887-95. DOI PubMed
35. Yam VW, Fung WK, Cheung K. Luminescence behavior of polynuclear alkynylcopper(I) Phosphines. *J Cluster Sci* 1999; 10:37-69. DOI
36. Vega A, Calvo V, Spodine E, Zárate A, Fuenzalida V, Saillard JY. A novel copper cobalt inorganometallic cluster. Synthesis, structure and bonding analysis of $Cu(_3)[mu(_2)-(CCHCo(_2)(CO)(_6))](_3)$. *Inorg Chem* 2002;41:3389-95. DOI PubMed
37. Tsipis AC, Tsipis CA. Hydrometal analogues of aromatic hydrocarbons: a new class of cyclic hydrocoppers(I). *J Am Chem Soc* 2003;125:1136-7. DOI PubMed
38. Boca R, Dlhán L, Mezei G, Ortiz-Pérez T, Raptis RG, Telser J. Triangular, ferromagnetically-coupled CuII 3-pyrazolato complexes as possible models of particulate methane monooxygenase (pMMO). *Inorg Chem* 2003;42:5801-3. DOI PubMed
39. Gawande MB, Goswami A, Felpin FX, et al. Cu and Cu-based nanoparticles: synthesis and applications in catalysis. *Chem Rev* 2016;116:3722-811. DOI PubMed
40. Bhanushali S, Ghosh P, Ganesh A, Cheng W. 1D copper nanostructures: progress, challenges and opportunities. *Small* 2015;11:1232-52. DOI PubMed
41. Yang L, Frauenheim T, Ganz E. Properties of the free-standing two-dimensional copper monolayer. *J Nanomater* 2016;2016:1-6. DOI
42. Yang LM, Bačić V, Popov IA, et al. Two-dimensional $Cu_2Si$ monolayer with planar hexacoordinate copper and silicon bonding. *J Am Chem Soc* 2015;137:2757-62. DOI PubMed
43. Feng B, Fu B, Kasamatsu S, et al. Experimental realization of two-dimensional Dirac nodal line fermions in monolayer $Cu_2Si$. *Nat Commun* 2017;8:1007. DOI PubMed PMC
44. Yan L, Liu P, Bo T, et al. Emergence of superconductivity in a Dirac nodal-line $Cu_2Si$ monolayer: ab initio calculations. *J Mater Chem C* 2019;7:10926-32. DOI
45. Ma Y, Kou L, Dai Y, Heine T. Two-dimensional topological insulators in group-11 chalcogenide compounds: $M_2Te$(M=Cu,Ag). *Phys Rev B* 2016:93. DOI
46. Yang LM, Popov IA, Boldyrev AI, Heine T, Frauenheim T, Ganz E. Post-anti-van't Hoff-Le Bel motif in atomically thin germanium-copper alloy film. *Phys Chem Chem Phys* 2015;17:17545-51. DOI PubMed
47. Li S, Ren G, Miao C, Jin Z. M4H4X: Hydrometals (M = Cu, Ni) containing tetracoordinate planar nonmetals (X=B, C, N, O). *Angew Chem* 2004;116:1395-7. DOI PubMed
48. Li S, Miao C, Ren G. $D_5h$ $Cu_5H_5X$: Pentagonal hydrocopper $Cu_5H_5$ containing pentacoordinate planar nonmetal centers (X = B, C, N, O). *Eur J Inorg Chem* 2004;2004:2232-4. DOI
49. Jia J, Zhang H, Wang Z, Zhao J, Zhou Z. A $Cu_2B_2$ monolayer with planar hypercoordinate motifs: an efficient catalyst for CO electroreduction to ethanol. *J Mater Chem A* 2020;8:9607-15. DOI
50. Weng X, He X, Hou J, et al. First-principles prediction of two-dimensional copper borides. *Phys Rev Materials* 2020:4. DOI

51. Yue C, Weng X, Gao G, et al. Formation of copper boride on Cu(111). *Fundam Res* 2021;1:482-7. DOI
52. Becke AD. Density-functional thermochemistry. III. The role of exact exchange. *J Chem Phys* 1993;98:5648-52. DOI
53. Lee C, Yang W, Parr RG. Development of the Colle-Salvetti correlation-energy formula into a functional of the electron density. *Phys Rev B Condens Matter* 1988;37:785-9. DOI PubMed
54. Stephens PJ, Devlin FJ, Chabalowski CF, Frisch MJ. Ab initio calculation of vibrational absorption and circular dichroism spectra using density functional force fields. *J Phys Chem* 1994;98:11623-7. DOI
55. Neese F. Software update: the ORCA program system, version 4.0. *WIREs Comput Mol Sci* 2018:8. DOI
56. Blöchl PE. Projector augmented-wave method. *Phys Rev B Condens Matter* 1994;50:17953-79. DOI PubMed
57. Kresse G, Joubert D. From ultrasoft pseudopotentials to the projector augmented-wave method. *Phys Rev B* 1999;59:1758-75. DOI
58. Kresse G, Hafner J. Ab initio molecular dynamics for liquid metals. *Phys Rev B Condens Matter* 1993;47:558-61. DOI PubMed
59. Perdew JP, Burke K, Ernzerhof M. Generalized gradient approximation made simple. *Phys Rev Lett* 1996;77:3865-8. DOI PubMed
60. Heyd J, Scuseria GE, Ernzerhof M. Hybrid functionals based on a screened Coulomb potential. *J Chem Phys* 2003;118:8207-15. DOI
61. Becke AD, Edgecombe KE. A simple measure of electron localization in atomic and molecular systems. *J Chem Phys* 1990;92:5397-403. DOI
62. Silvi B, Savin A. Classification of chemical bonds based on topological analysis of electron localization functions. *Nature* 1994;371:683-6. DOI
63. Galeev TR, Dunnington BD, Schmidt JR, Boldyrev AI. Solid state adaptive natural density partitioning: a tool for deciphering multi-center bonding in periodic systems. *Phys Chem Chem Phys* 2013;15:5022-9. DOI PubMed
64. Clark SJ, Segall MD, Pickard CJ, et al. First principles methods using CASTEP. *Z Kristallogr - Cryst Mater* 2005;220:567-70. DOI
65. Segall MD, Shah R, Pickard CJ, Payne MC. Population analysis of plane-wave electronic structure calculations of bulk materials. *Phys Rev B* 1996; 54:16317-16320. DOI PubMed
66. Togo A, Tanaka I. First principles phonon calculations in materials science. *Scr Mater* 2015;108:1-5. DOI
67. Martyna GJ, Klein ML, Tuckerman M. Nosé-Hoover chains: the canonical ensemble via continuous dynamics. *J Chem Phys* 1992;97:2635-43. DOI
68. Giannozzi P, Baroni S, Bonini N, et al. QUANTUM ESPRESSO: a modular and open-source software project for quantum simulations of materials. *J Phys Condens Matter* 2009;21:395502. DOI PubMed
69. Savrasov SY, Savrasov DY, Andersen OK. Linear-response calculations of electron-phonon interactions. *Phys Rev Lett* 1994;72:372-5. DOI PubMed
70. Kurth S, Marques M, Lüders M, Gross EKU. Local density approximation for superconductors. *Phys Rev Lett* 1999;83:2628-31. DOI
71. Moret ME, Zhang L, Peters JC. A polar copper-boron one-electron σ-bond. *J Am Chem Soc* 2013;135:3792-5. DOI PubMed
72. Holler S, Tüchler M, Belaj F, Veiros LF, Kirchner K, Mösch-Zanetti NC. Thiopyridazine-based copper boratrane complexes demonstrating the Z-type nature of the ligand. *Inorg Chem* 2016;55:4980-91. DOI PubMed
73. Wang Y, Quillian B, Wei P, et al. A stable, neutral diborene containing a B=B double bond. *J Am Chem Soc* 2007;129:12412-3. DOI PubMed
74. Zhou M, Tsumori N, Li Z, Fan K, Andrews L, Xu Q. OCBBCO: a neutral molecule with some boron-boron triple bond character. *J Am Chem Soc* 2002;124:12936-7. DOI PubMed
75. Braunschweig H, Dewhurst RD, Hammond K, Mies J, Radacki K, Vargas A. Ambient-temperature isolation of a compound with a boron-boron triple bond. *Science* 2012;336:1420-2. DOI PubMed
76. Wiberg K. Application of the pople-santry-segal CNDO method to the cyclopropylcarbinyl and cyclobutyl cation and to bicyclobutane. *Tetrahedron* 1968;24:1083-96. DOI
77. Harper LK, Shoaf AL, Bayse CA. Predicting trigger bonds in explosive materials through wiberg bond index analysis. *Chem Phys Chem* 2015; 16:3886-3892. DOI PubMed
78. Mayer I. Bond order and valence indices: a personal account. *J Comput Chem* 2007;28:204-21. DOI PubMed
79. Foster JP, Weinhold F. Natural hybrid orbitals. *J Am Chem Soc* 1980;102:7211-8. DOI PubMed
80. Reed AE, Weinhold F. Natural bond orbital analysis of near-Hartree-Fock water dimer. *J Chem Phys* 1983;78:4066-73. DOI
81. Hoffmann R, Alder RW, Wilcox CF. Planar tetracoordinate carbon. *J Am Chem Soc* 1970;92:4992-3. DOI
82. Reed AE, Weinstock RB, Weinhold F. Natural population analysis. *J Chem Phys* 1985;83:735-46. DOI
83. Hirshfeld FL. Bonded-atom fragments for describing molecular charge densities. *Theoret Chim Acta* 1977;44:129-38. DOI
84. Lee C, Wei X, Kysar JW, Hone J. Measurement of the elastic properties and intrinsic strength of monolayer graphene. *Science* 2008; 321:385-388. DOI PubMed
85. Cai Y, Zhang G, Zhang YW. Polarity-reversed robust carrier mobility in monolayer MoS□ nanoribbons. *J Am Chem Soc* 2014;136:6269-75. DOI PubMed
86. Wei X, Fragneaud B, Marianetti CA, Kysar JW. Nonlinear elastic behavior of graphene: Ab initio calculations to continuum description. *Phys Rev B* 2009:80. DOI
87. Peng Q, Ji W, De S. Mechanical properties of the hexagonal boron nitride monolayer: Ab initio study. *Comput Materi Sci* 2012;56:11-7. DOI
88. Cooper RC, Lee C, Marianetti CA, Wei X, Hone J, Kysar JW. Nonlinear elastic behavior of two-dimensional molybdenum disulfide. *Phys Rev B* 2013:87. DOI
89. Nagamatsu J, Nakagawa N, Muranaka T, Zenitani Y, Akimitsu J. Superconductivity at 39K in magnesium diboride. *Nature*

2001;410:63-4. DOI PubMed

90. Kortus J, Mazin II, Belashchenko KD, Antropov VP, Boyer LL. Superconductivity of metallic boron in $MgB_2$. *Phys Rev Lett* 2001;86:4656-9. DOI PubMed
91. Allen PB, Dynes RC. Transition temperature of strong-coupled superconductors reanalyzed. *Phys Rev B* 1975;12:905-22. DOI
92. Chen J, Ge Y. Emergence of intrinsic superconductivity in monolayer $W_2N_3$. *Phys Rev B* 2021:103. DOI
93. Singh S, Romero AH, Mella JD, et al. High-temperature phonon-mediated superconductivity in monolayer $Mg_2B_4C_2$. *npj Quantum Mater* 2022:7. DOI
94. Zhang X, Zhou Y, Cui B, Zhao M, Liu F. Theoretical discovery of a superconducting two-dimensional metal-organic framework. *Nano Lett* 2017;17:6166-70. DOI PubMed
95. Bud'ko SL, Lapertot G, Petrovic C, Cunningham CE, Anderson N, Canfield PC. Boron isotope effect in superconducting $MgB_2$. *Phys Rev Lett* 2001;86:1877-80. DOI PubMed
96. Ge Y, Guan S, Liu Y. Two dimensional superconductors in electrides. *New J Phys* 2017;19:123020. DOI
97. Wang L, Xu C, Liu Z, et al. Magnetotransport properties in high-quality ultrathin two-dimensional superconducting $Mo_2C$ crystals. *ACS Nano* 2016;10:4504-10. DOI PubMed
98. Song B, Zhou Y, Yang HM, et al. Two-dimensional anti-van't hoff/Le Bel array $AlB_6$ with high stability, unique motif, triple dirac cones, and superconductivity. *J Am Chem Soc* 2019;141:3630-40. DOI PubMed
99. Peng R, Shen XP, Xie X, et al. Measurement of an enhanced superconducting phase and a pronounced anisotropy of the energy gap of a strained FeSe single layer in FeSe/Nb:$SrTiO_3$/$KTaO_3$ heterostructures using photoemission spectroscopy. *Phys Rev Lett* 2014;112:107001. DOI PubMed